nature nanotechnology

LETTERS

PUBLISHED ONLINE: 25 MARCH 2012 | DOI: 10.1038/NNANO.2012.35

Stable cycling of double-walled silicon nanotube battery anodes through solid–electrolyte interphase control

Hui Wu[1‡], Gerentt Chan[2‡], Jang Wook Choi[1†], Ill Ryu[1], Yan Yao[1], Matthew T. McDowell[1], Seok Woo Lee[1], Ariel Jackson[1], Yuan Yang[1], Liangbing Hu[1] and Yi Cui[1,3]*

Although the performance of lithium ion-batteries continues to improve, their energy density and cycle life remain insufficient for applications in consumer electronics, transport and large-scale renewable energy storage[1–5]. Silicon has a large charge storage capacity and this makes it an attractive anode material, but pulverization during cycling and an unstable solid–electrolyte interphase has limited the cycle life of silicon anodes to hundreds of cycles[6–11]. Here, we show that anodes consisting of an active silicon nanotube surrounded by an ion-permeable silicon oxide shell can cycle over 6,000 times in half cells while retaining more than 85% of their initial capacity. The outer surface of the silicon nanotube is prevented from expansion by the oxide shell, and the expanding inner surface is not exposed to the electrolyte, resulting in a stable solid–electrolyte interphase. Batteries containing these double-walled silicon nanotube anodes exhibit charge capacities approximately eight times larger than conventional carbon anodes and charging rates of up to 20C (a rate of 1C corresponds to complete charge or discharge in one hour).

Increasing the energy density of lithium-ion batteries requires the development of electrode materials with higher charge capacity or electrode materials with higher voltage[1–5], while improving the cycle life involves stabilizing two critical components of battery electrodes—the active electrode materials and their interface with the electrolyte (the so-called 'solid–electrolyte interphase', SEI). Recently, silicon has emerged as one of the most promising high-energy electrode materials, because it offers an appropriate low voltage for an anode and a high theoretical specific capacity of ~4,200 mAh g^{-1}, which is ten times higher than that of conventional carbon anodes[7–13]. However, silicon expands volumetrically by up to 400% on full lithium insertion (lithiation), and it can contract significantly on lithium extraction (delithiation)[6,11], creating two critical challenges: minimizing the degradation of the mechanical integrity of the silicon electrodes and maintaining the stability of the SEI.

Stress induced by large changes in the volume of silicon anodes causes cracking and pulverization, and in early studies of such anodes[6–11], this was considered to be the main reason for their rapid capacity loss. Recently, Verbrugge and co-workers suggested that the tendency for fracture and decrepitation could be reduced or avoided by reducing the material size to the nanometre range[14–17]. Indeed, the strain in such silicon nanostructures can be relaxed easily, without mechanical fracture, because of their small size and the available surrounding free space. Consistent with this theory, there has been some success in addressing material stability issues by designing nanostructured silicon materials including nanowires, nanotubes, nanoporous films and silicon nanoparticle/carbon composites[18–26]. This nanostructuring strategy has greatly increased the cycle life of silicon anodes to up to a few hundred cycles with 80% capacity retention[24,25], although this is still far from the desired cycle life of thousands of cycles.

SEI stability at the interface between the silicon and the liquid electrolyte is another critical factor in achieving a long cycle life. This is very challenging, and has not been effectively addressed for materials undergoing large volume changes, as shown in the schematic in Fig. 1. Electrolyte decomposition occurs due to the low potential of the anode and forms a passivating SEI layer on the electrode surface during battery charging. The SEI layer is an electronic insulator, but a lithium-ion conductor, so the growth of the SEI layer eventually terminates at a certain thickness[27,28]. Even though mechanical fracture issues are largely overcome by using silicon nanostructures, their interface with the electrolyte is not static due to their repetitive volume expansion and contraction[6,8,12,26]. As is schematically shown in Fig. 1a,b, both the solid and hollow silicon structures expand out towards the electrolyte upon lithiation, then contract during delithiation. The SEI formed in the lithiated expanded state can be broken as the nanostructure shrinks during delithiation. This re-exposes the fresh silicon surface to the electrolyte and the SEI forms again, resulting in the SEI becoming thicker with each charge/discharge cycle. This results in a degradation in battery performance through (i) the consumption of electrolyte and lithium ions during continuous SEI formation; (ii) the electrically insulating nature of the SEI weakening the electrical contact between the current collector and anode material; (iii) the long lithium diffusion distance through the thick SEI; and (iv) electrode material degradation caused by mechanical stress from the thick SEI. The formation of a stable SEI is critical for realizing a long cycle life in silicon anodes; this also holds generally for other electrode materials subject to large volume changes.

Here we design a novel double-walled Si–SiO_x nanotube (DWSiNT) anode, in which the inner wall is active silicon and the outer wall is confining SiO_x, which allows lithium ions to pass through (see the cross-sectional view in Fig. 1c). In this design, the electrolyte only contacts the outer surface and cannot enter the inner hollow space. During lithiation, lithium ions penetrate through the outer wall and react with the inner silicon wall. The outer wall is mechanically rigid, so the inner silicon wall expands

[1]Department of Materials Science and Engineering, Stanford University, California 94305, USA, [2]Department of Chemistry, Stanford University, California 94305, USA, [3]Stanford Institute for Materials and Energy Sciences, SLAC National Accelerator Laboratory, Menlo Park, California 94205, USA; [†]Present address: Graduate School of EEWS, Korea Advanced Institute of Science and Technology, Daejeon 305-701, Republic of Korea; [‡]These authors contributed equally to this work. *e-mail: yicui@stanford.edu

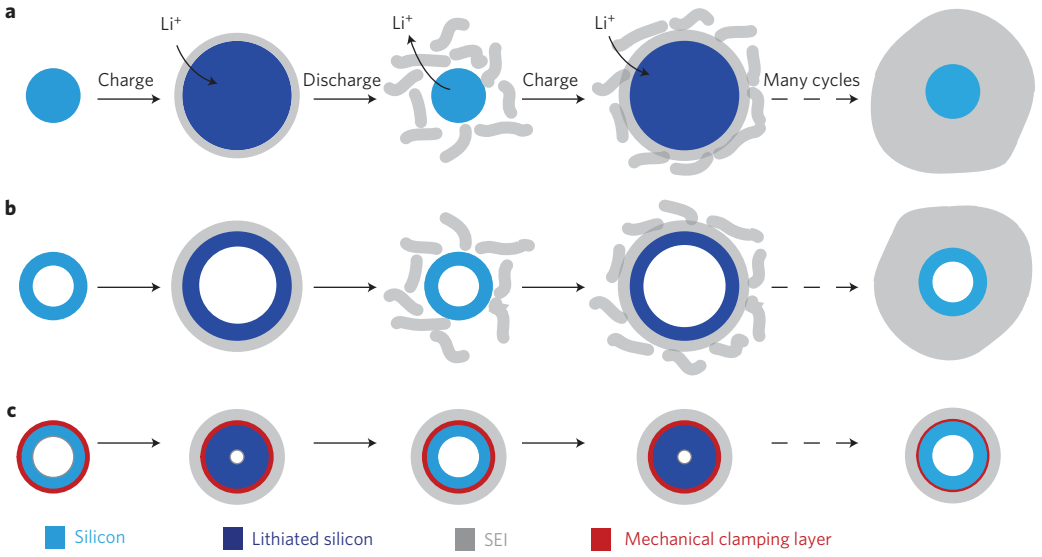

Figure 1 | Schematic of SEI formation on silicon surfaces. a, A solid silicon nanowire expands upon lithiation. A thin layer of SEI forms in this lithiated and expanded state. During delithiation, the silicon structures shrink, and the SEI can break down into separate pieces, exposing fresh silicon surface to the electrolyte. In later cycles, new SEI continues to form on the newly exposed silicon surfaces, and this finally results in a very thick SEI layer on the outside of the silicon nanowires. **b**, Similarly, a thick SEI grows outside the silicon nanotube without a mechanical constraining layer, which also has a varying and unstable interface with the electrolyte. **c**, Designing a mechanical constraining layer on the hollow silicon nanotubes can prevent silicon from expanding outside towards the electrolyte during lithiation. As a result, a thin and stable SEI can be built.

inward into the hollow space. This inward expansion is possible because silicon is considerably softened on significant lithium insertion. During delithiation, the inner surface of the silicon wall shrinks back. Overall, the interface with the electrolyte is mechanically constrained and remains static during both lithiation and delithiation. Only the inner surface moves back and forth, and it does not contact the electrolyte. The DWSiNT structure provides two attractive features as an anode material: (i) the static outer surface allows for the development of a stable SEI; (ii) the inner space allows for free volume expansion of the silicon without mechanical breaking (Fig. 1c).

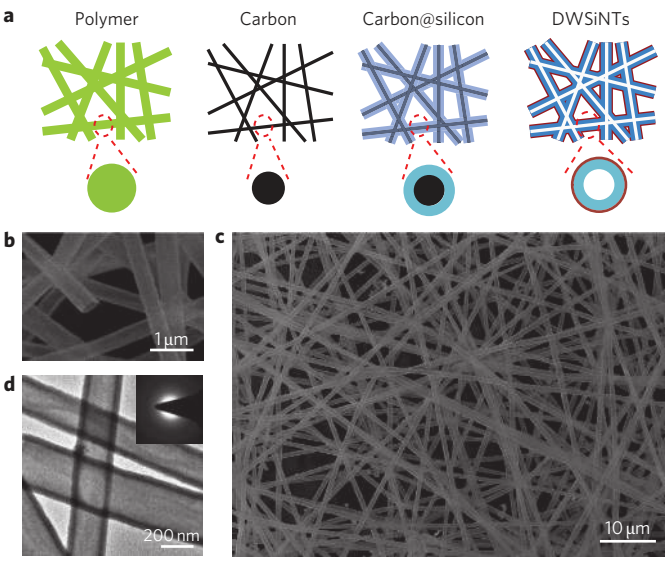

Figure 2 | Fabrication and characterization of DWSiNTs. a, Schematic of the fabrication process for DWSiNTs. Polymer nanofibres (green) were first made by electrospinning. The polymer fibres were then carbonized and coated with silicon (blue) using a CVD method. By heating the sample in air at 500 °C, the inner carbon templates (black) were selectively removed, leaving continuous silicon tubes with a SiO_x mechanical constraining layer (red). **b**,**c**, SEM images of synthesized DWSiNTs at high and low magnification, respectively. **d**, TEM image of DWSiNTs, showing the uniform hollow structure with smooth tube walls.

We developed an electrospun nanofibre templating method to experimentally realize the DWSiNTs (schematically shown in Fig. 2a). A detailed explanation of the synthetic procedures is given in the Methods. Figure 2b presents a scanning electron microscope (SEM) image of the synthesized materials, demonstrating that smooth and uniform hollow tubes were fabricated with full removal of their inner cores. The low-magnification SEM image in Fig. 2c shows that the synthesized tubes were continuous over long distances. This continuous tube structure is vital for preventing the electrolyte from wetting the interior, thus protecting the tubes from undergoing SEI interior growth (discussed later). Another advantage of this continuous network of nanotubes is to provide mechanical and electrical interconnects throughout the entire network, thus making it possible to use free-standing nanotube mats directly as battery anodes, without any conducting additives or binders. A transmission electron microscope (TEM) image of the synthesized tubes (Fig. 2d) shows that both the inside and outside surfaces are smooth and the wall thickness is 30 nm. A selected area electron diffraction (SAED) pattern shows diffuse scattering (Fig. 2d, inset), suggesting that the synthesized nanotubes are amorphous.

It is important to note that the outside surfaces of the tubes, which were heated in air at 500 °C during the carbon-removal process, have been oxidized naturally, forming a thin, external coating of silicon oxide. During oxidation of the existing carbon core, there is very little oxidation of the inner surface of the silicon tubes because the carbon core is a sacrificial material and consumes oxygen first. Therefore, we expect that the proposed DWSiNT structure can be formed with the outer wall comprising SiO_x and the inner wall silicon. To confirm this, Auger electron spectroscopy sputter depth profiling was performed to assess the elemental distribution along the cross-section of the DWSiNTs (Supplementary Fig. S3).

Both our mechanical simulation and our *ex situ* TEM study confirmed that oxide-free silicon nanotubes expand outwards during lithiation, whereas the oxide wall of DWSiNTs forces the silicon

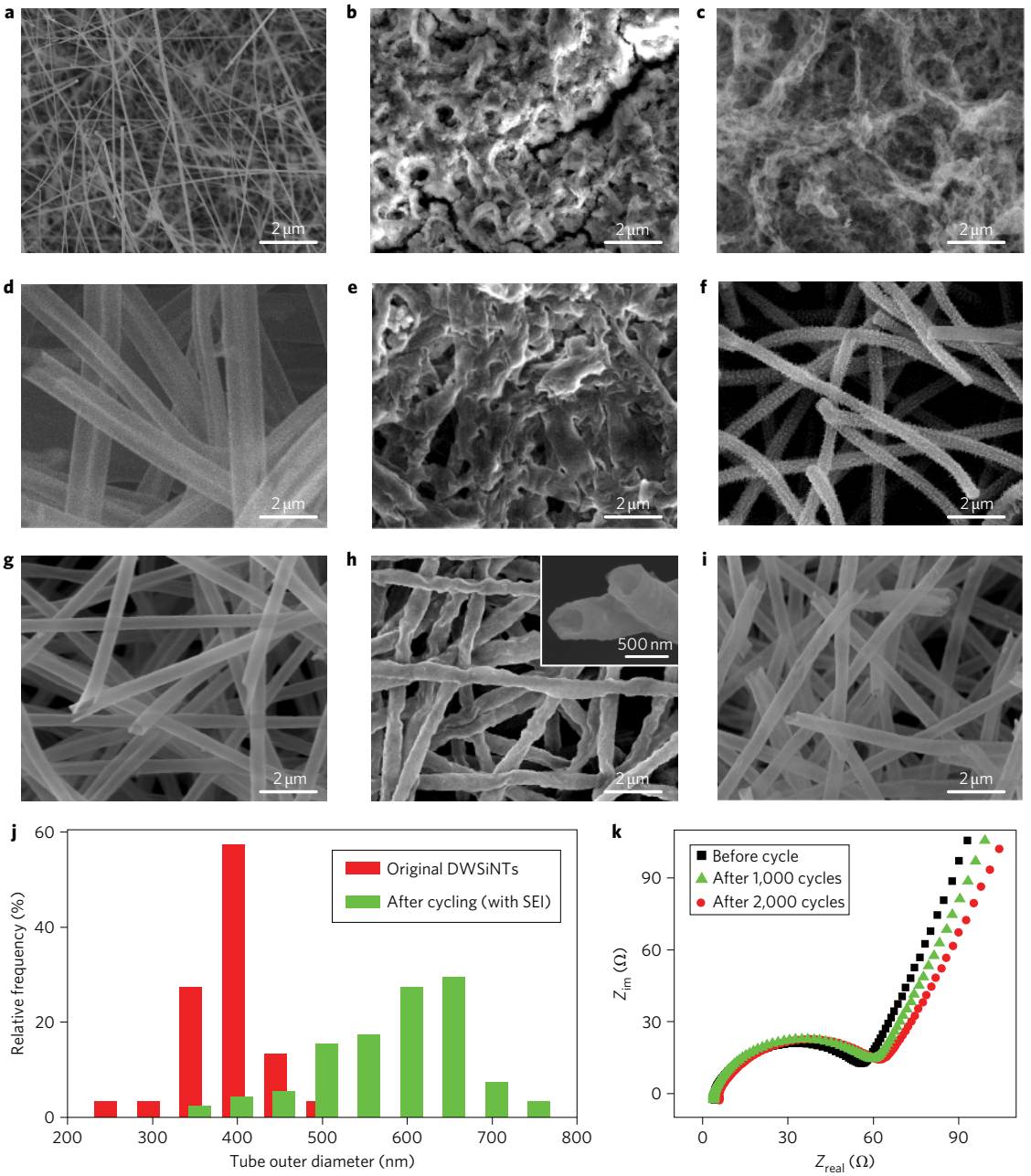

Figure 3 | SEI formation on silicon electrodes with different nanostructures. a–i, SEM images of different silicon nanostructures before and after cycling. SEM images of initial silicon nanowires (**a**), silicon nanotubes (**d**) and DWSiNTs (**g**), respectively. SEM images of silicon nanowires (**b**) and silicon nanotubes (**e**) after 200 cycles; a thick SEI layer can be seen covering the nanostructures. DWSiNTs after 2,000 cycles (**h**), showing the tubes coated with a uniform thin SEI layer. SEM images of nanowires (**c**), nanotubes (**f**) and DWSiNTs (**i**) after cycling 200, 200 and 2,000 times, respectively. In these images, the SEI was selectively removed by chemical etching. **j**, Statistical analysis of DWSiNT diameters before and after 2,000 cycles. The average diameters of the initial tubes and cycled tubes are 400 nm and 620 nm, indicating an average SEI thickness of 110 nm. **k,** Impedance measurements for DWSiNTs after different numbers of cycles.

to expand inwards only (Supplementary Figs S5–S8, Table S1 and discussion). This mechanical constraining effect in DWSiNTs provides a very exciting ability to control the SEI. To demonstrate this experimentally, we prepared battery cells in which three different types of silicon nanostructured electrodes were paired with lithium foil in half cells: (i) solid silicon nanowires (Fig. 3a); (ii) hollow silicon nanotubes without the SiO_x clamping layer (Fig. 3d) and (iii) hollow DWSiNTs with the SiO_x clamping layer (Fig. 3g). These silicon electrodes were subjected to deep cycling (1 V–0.01 V) and then extracted for observation with SEM (200 cycles for the silicon nanowires and single-walled silicon nanotubes without the clamping layer, and 2,000 cycles for DWSiNTs). After 200 cycles, both the silicon nanowires and silicon nanotubes without the clamping layer can be seen to be buried under SEI layers, showing that the SEI has grown very thick (Fig. 3b,e). However, the situation for the DWSiNTs is very different. Even after many more cycles (2,000), the DWSiNTs only have a very thin SEI layer and individual DWSiNTs (with an SEI coating) can be clearly resolved (Fig. 3h). A statistical analysis shows that the outer diameters of the DWSiNTs increase only slightly after cycling (Fig. 3j), and the SEI layer thickness is calculated to be only ~110 nm. This

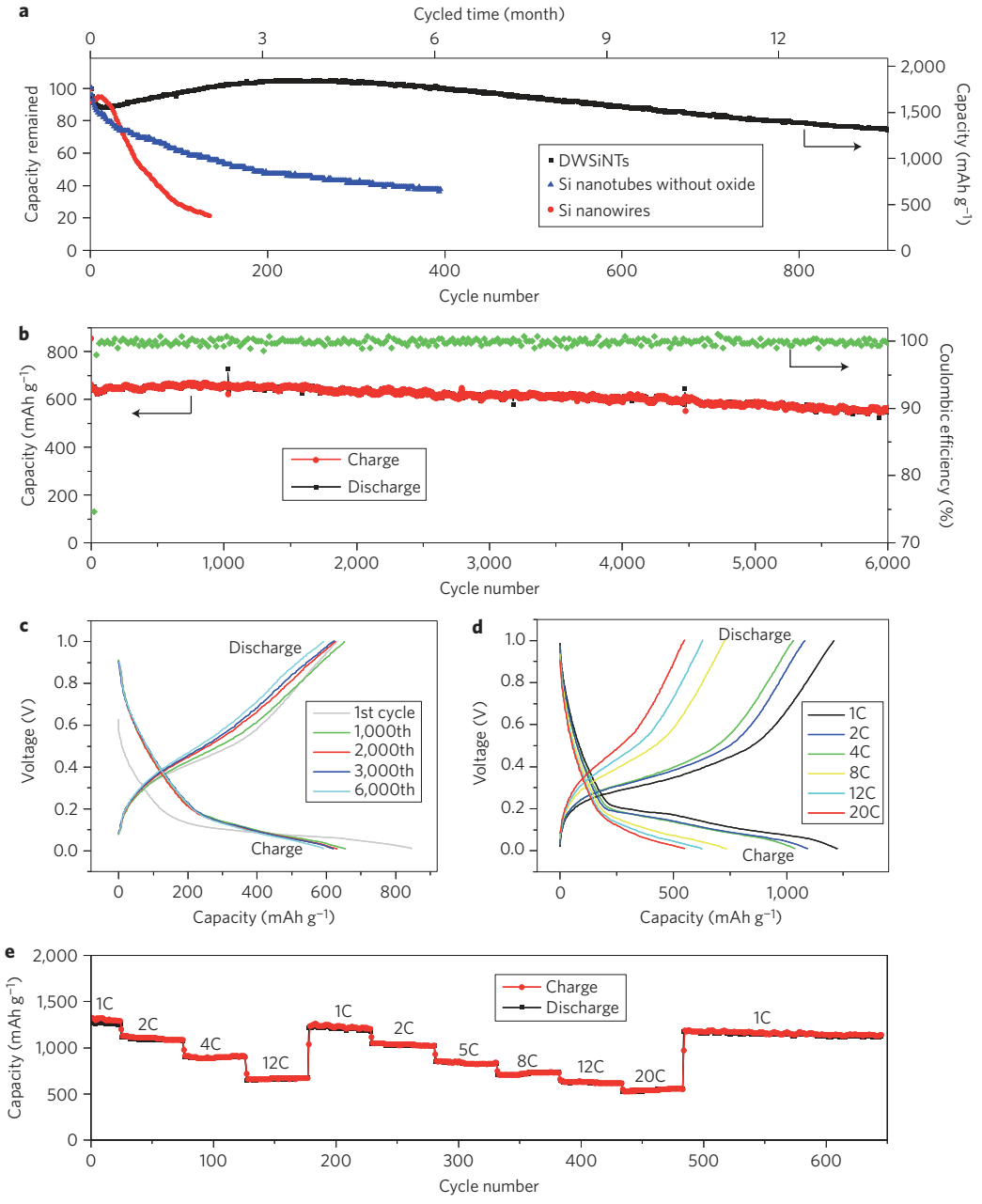

Figure 4 | Electrochemical characteristics of DWSiNTs tested between 1 V and 0.01 V. a, Capacity retention of different silicon nanostructures. All samples were cycled at the same charge/discharge rate of C/5. The calendar life and delithiation capacity of DWSiNTs can also be seen in this figure. **b**, Lithiation/delithiation capacity and CE of DWSiNTs cycled at 12C for 6,000 cycles. There is no significant capacity fading after 6,000 cycles. **c**, Voltage profiles plotted for the 1st, 1,000th, 2,000th, 3,000th and 6,000th cycles. **d**,**e**, Galvanostatic charge/discharge profiles (**d**) and capacity (**e**) of DWSiNTs cycled at various rates from 1C to 20C. All electrochemical measurements (**a**–**e**) were carried out at room temperature in two-electrode 2032 coin-type half-cells. All the specific capacities of DWSiNTs are reported based on the total weight of Si–SiO_x.

thickness is similar to the thickness of SEI formed on an excellent carbon anode. It is important to note that due to the continuous structure of the tubes, the electrolyte does not wet the inside of the tubes even if there is a capillary force present, which can be confirmed by direct observation of a DWSiNT after immersing in electrolyte and drying (Supplementary Fig. S9). Also, the lack of electrolyte wetting inside the tubes does not allow for SEI formation there. To demonstrate this, we used a focused ion beam to slice open the DWSiNTs after cycling. Supplementary Fig. S10 presents SEM images of cycled DWSiNTs after slicing; these images clearly show that there is no SEI formation inside the hollow space of the DWSiNTs.

Silicon material stability is also important for battery cycling, so we compared changes in silicon morphology for these three types of nanostructures. We previously developed an acid etching method to remove the SEI without damaging the silicon electrode materials[29]. On SEI removal using this technique, the nanowires and nanotubes without the oxide layer could be seen to have very rough and highly porous surfaces (Fig. 3c,f, respectively), indicating significant material displacement and morphological changes[29]. However, after removing the SEI from the DWSiNTs, they still appear smooth, continuous and uniform (Fig. 3i), similar to those before cycling. This further suggests that the silicon material is stable, with the outer surface undergoing very little change during

cycling and remaining static. The controlled thin SEI growth on DWSiNTs can be beneficial for the cell impedance in batteries. Rapid SEI growth can easily result in an increase in the impedance in electrodes, as well as a decrease in capacity with cycling[30,31]. To further confirm this controlled SEI growth on DWSiNTs, we performed cell impedance tests of the DWSiNTs electrode before cycling and after 1,000 and 2,000 cycles. As shown in Fig. 3k, no obvious impedance increase was detected, indicating no significant growth of SEI during cycling.

The stable materials and SEI of DWSiNTs should afford an excellent cycle life under deep charge/discharge cycling (Fig. 4). The specific capacity values reported in Fig. 4 are calculated on the basis of the total weight of Si–SiO_x, in which silicon comprises ~60% of the total DWSiNT mass (see Methods for weight determination). The specific reversible lithium extraction capacity of the DWSiNTs reached 1,780 mAh g^{-1} at a rate of C/5 (current density 0.4 A g^{-1}, Fig. 4a). The volumetric capacity of the tube electrode can be up to ~2 Ah cm^{-3}. The gravimetric capacity of silicon alone is estimated to be very high, at ~2,791 mAh g^{-1}. The cycling performance of three different types of silicon electrodes with different SEI formation behaviour is compared in Fig. 4a for C/5 deep charge/discharge cycling. Under such a deep charge/discharge from 1 V to 0.01 V, fast capacity fading for anodes made from silicon nanowires (red) and nanotubes without the constraining oxide (blue) can be observed. For DWSiNT samples (black), no capacity decay was detected after 300 cycles, capacity retention after 500 cycles was 94%, and 76% of the initial discharge capacity remained after 900 cycles. Note that it takes more than one year to complete 900 cycles at the C/5 rate, and the fading here might have resulted from electrolyte leakage in the battery over such a long time. The initial increase of DWSiNT capacity in Fig. 4a is due to the slight increase in room temperature from winter to spring during cycling. To obtain ultralong cycling results within a reasonable time period, faster charge and discharge tests were also carried out. Significantly, the DWSiNT anode cycled at a rate of 10C retains 93% of its initial capacity after 4,000 cycles and 88% after 6,000 cycles (Fig. 4b). The voltage profiles of the different cycles are shown in Fig. 4c. The lithiation potential shows a sloping profile between 0.1 and 0.01 V, consistent with the behaviour of amorphous silicon[19,20]. No obvious change in charge/discharge profile can be found after 6,000 cycles for the DWSiNT anode, indicating superior and stable cycling performance. This extremely long cycle life can be attributed to the stable SEI and materials in the DWSiNTs.

Coulombic efficiency (CE) is another important concern for silicon. For 5,000 cycles of operation in a full cell, the CE for a silicon half cell must exceed 99.994%. For our electrode, the CE of the first cycle was 76%, because the constraining SiO_x layer and initial SEI formation consume some lithium, although this could be improved by pre-lithiation in future studies. The stability of the SEI layer helps to achieve a high CE after the first cycle (Fig. 4b). The average CE of the DWSiNTs electrode for cycles from the 2nd to 6,000th is 99.938%, which is much higher than for silicon nanoparticles and nanowires[32], but still lower than required (>99.994% for 5,000 cycles in a full cell). This CE can probably be improved by surface treatments and electrolyte modifications[13,32]. The thin tube side wall is important for maintaining a high stability of the electrochemical properties due to the limited clamping force of the surface oxide layer. DWSiNTs with thicker silicon side walls will lose the constraining effect, and therefore have lower cycling stabilities (Supplementary Fig. S11). In addition, the thin and stable SEI and the nanoscale thickness of the walls in DWSiNTs can also enable outstanding high power rate capability. Between 1C and 20C, for the silicon alone, high and stable capacities between ~1,880 mAh g^{-1} and ~850 mAh g^{-1} were demonstrated in the DWSiNTs (equivalent to between 1,200 and 540 mAh g^{-1} based on total DWSiNT weight). Clearly, lithium ions can rapidly pass through the thin SEI layer and constraining oxide to reach the silicon active material, even at very high C rates.

In summary, we have designed a DWSiNT structure to successfully address the silicon material and SEI stability issues, and we have demonstrated its use as a high-performance anode with long cycle life (6,000 cycles with 88% capacity retention), high specific charge capacity (~2,971/1,780 mAh g^{-1} at C/5, ~940/600 mAh g^{-1} at 12C; capacity based on silicon/total-DWSiNT weight, respectively) and fast charge/discharge rates (up to 20C). These performance parameters can be applied to the next generation of high-performance batteries for portable electronics, electric vehicles and grid-scale applications. This successful materials design for silicon-based anodes could also be extended to other high-capacity anode and cathode materials systems that undergo large volume expansion.

Methods

We used a templating method to synthesize the DWSiNTs, as schematically shown in Fig. 2a. Polymer nanofibres were first produced by electrospinning, a well-known technique for making continuous ultralong nanofibres at low cost and in large quantities[33,34]. Electrospinning solution was made by adding 1.0 g of polyacrylonitrile (PAN) to 9.0 g of dimethyl formamide (both from Sigma-Alrich) and stirred at 70 °C for 1 h. We used a commercial high-voltage source (Gamma High Voltage Research, model ES-30P-5W) for electrospinning. A voltage of 15 kV was applied to the solution to start the spinning process, and the electrospun fibres were collected in a random mat of approximately 10 cm × 10 cm. A large quantity of PAN nanofibres could be produced within several minutes of processing time.

The polymer fibres were pre-carbonized by heating in air at a rate of 1 °C min^{-1} to 280 °C and held for 5 h. The sample was then placed in a tube furnace and carbonized by heating in argon (g) at a rate of 10 °C min^{-1} and held at 500 °C for 0.5 h (Supplementary Fig. S1). Using a SiH_4 chemical vapour deposition (CVD) method, a thin layer (~30 nm) of silicon was coated onto the carbon nanofibres at 490 °C (Supplementary Fig. S2). The free-standing carbon nanofibres coated with silicon were then heated in air at 500 °C for 2 h. Oxygen gas could diffuse through the broken ends of the nanofibres, and the carbon cores were oxidized into carbon dioxide gas and removed completely. A SiO_x layer outside the silicon nanotubes formed during this oxidation process. The weight ratio between silicon and SiO_x was determined by measuring the weight loss in the DWSiNTs after removing the SiO_x layer by washing in HF.

The electrochemical properties were evaluated by galvanostatic cycling of coin cells with the interconnected hollow silicon nanotube networks as the working electrode and lithium foil as the counter/reference electrode. The testing electrode was made by laminating a freestanding silicon nanotube mat on copper foil; the mass loading was 0.02–0.1 mg cm^{-2} and no binders or conducting carbon were used. The electrolyte for all tests was 1 M $LiPF_6$ in ethylene carbonate/diethyl carbonate (1:1 v/v, Ferro Corporation), and separators from Asahi Kasei were used. All cells were cycled between 0.01 and 1 V.

Received 19 December 2011; accepted 21 February 2012; published online 25 March 2012

References

1. Armand, M. & Tarascon, J. M. Building better batteries. *Nature* **451,** 652–657 (2008).
2. Goodenough, J. B. & Kim, Y. Challenges for rechargeable Li batteries. *Chem. Mater.* **22,** 587–603 (2009).
3. Kang, B. & Ceder, G. Battery materials for ultrafast charging and discharging. *Nature* **458,** 190–193 (2009).
4. Whittingham, M. S. Lithium batteries and cathode materials. *Chem. Rev.* **104,** 4271–4301 (2004).
5. Tarascon, J. M. & Armand, M. Issues and challenges facing rechargeable lithium batteries. *Nature* **414,** 359–367 (2001).
6. Beaulieu, L. Y., Eberman, K. W., Turner, R. L., Krause, L. J. & Dahn, J. R. Colossal reversible volume changes in lithium alloys. *Electrochem. Solid State Lett.* **4,** A137–A140 (2001).
7. Besenhard, J. O., Yang, J. & Winter, M. Will advanced lithium-alloy anodes have a chance in lithium-ion batteries? *J. Power Sources* **68,** 87–90 (1997).
8. Hatchard, T. D. & Dahn, J. R. *In situ* XRD and electrochemical study of the reaction of lithium with amorphous silicon. *J. Electrochem. Soc.* **151,** A838–A842 (2004).
9. Raimann, P. R. *et al.* Monitoring dynamics of electrode reactions in Li-ion batteries by *in situ* ESEM. *Ionics* **12,** 253–255 (2006).
10. Weydanz, W. J., Wohlfahrt-Mehrens, M. & Huggins, R. A. A room temperature study of the binary lithium–silicon and the ternary lithium–chromium–silicon system for use in rechargeable lithium batteries. *J. Power Sources* **81,** 237–242 (1999).

11. Zhang, X. W. *et al.* Electrochemical performance of lithium ion battery, nano-silicon-based, disordered carbon composite anodes with different microstructures. *J. Power Sources* **125,** 206–213 (2004).
12. Beaulieu, L. Y., Hatchard, T. D., Bonakdarpour, A., Fleischauer, M. D. & Dahn, J. R. Reaction of Li with alloy thin films studied by *in situ* AFM. *J. Electrochem. Soc.* **150,** A1457–A1464 (2003).
13. Zhang, W. J. A review of the electrochemical performance of alloy anodes for lithium-ion batteries. *J. Power Sources* **196,** 13–24 (2011).
14. Deshpande, R., Cheng, Y. T. & Verbrugge, M. W. Modeling diffusion-induced stress in nanowire electrode structures. *J. Power Sources* **195,** 5081–5088 (2010).
15. Verbrugge, M. W. & Cheng, Y. T. Stress and strain-energy distributions within diffusion-controlled insertion-electrode particles subjected to periodic potential excitations. *J. Electrochem. Soc.* **156,** A927–A937 (2009).
16. Cheng, Y. T. & Verbrugge, M. W. The influence of surface mechanics on diffusion induced stresses within spherical nanoparticles. *J. Appl. Phy.* **104,** 083521 (2008).
17. Verbrugge, M. W., Cheng, Y. T. Stress distribution within spherical particles undergoing electrochemical insertion and extraction. *Electrochem. Soc. Trans.* **13,** 127–139 (2008).
18. Chan, C. K. *et al.* High-performance lithium battery anodes using silicon nanowires. *Nature Nanotech.* **3,** 31–35 (2008).
19. Cui, L. F., Ruffo, R., Chan, C. K., Peng, H. L. & Cui, Y. Crystalline–amorphous core–shell silicon nanowires for high capacity and high current battery electrodes. *Nano Lett.* **9,** 491–495 (2009).
20. Cui, L. F., Yang, Y., Hsu, C. M. & Cui, Y. Carbon–silicon core–shell nanowires as high capacity electrode for lithium ion batteries. *Nano Lett.* **9,** 3370–3374 (2009).
21. Hertzberg, B., Alexeev, A. & Yushin, G. Deformations in Si–Li anodes upon electrochemical alloying in nano-confined space. *J. Am. Chem. Soc.* **132,** 8548–8549 (2010).
22. Kim, H., Han, B., Choo, J. & Cho, J. Three-dimensional porous silicon particles for use in high-performance lithium secondary batteries. *Angew. Chem. Int. Ed.* **47,** 10151–10154 (2008).
23. Kim, H., Seo, M., Park, M. H. & Cho, J. A Critical size of silicon nano-anodes for lithium rechargeable batteries. *Angew. Chem. Int. Ed.* **49,** 2146–2149 (2008).
24. Magasinski, A. *et al.* High-performance lithium-ion anodes using a hierarchical bottom-up approach. *Nature Mater.* **9,** 353–358 (2010).
25. Park, M. H. *et al.* Silicon nanotube battery anodes. *Nano Lett.* **9,** 3844–3847 (2009).
26. Song, T. *et al.* Arrays of sealed silicon nanotubes as anodes for lithium ion batteries. *Nano Lett.* **10,** 1710–1716 (2010).
27. Aurbach, D. Review of selected electrode–solution interactions which determine the performance of Li and Li ion batteries. *J. Power Sources* **89,** 206–218 (2000).
28. Verma, P., Maire, P. & Novak, P. A review of the features and analyses of the solid electrolyte interphase in Li-ion batteries. *Electrochem. Acta* **55,** 6332–6341 (2010).
29. Choi, J. W. *et al.* Stepwise nanopore evolution in one-dimensional nanostructures. *Nano Lett.* **10,** 1409–1413 (2010).
30. Chan, C. K., Ruffo, R., Hong, S. S. & Cui, Y. Surface chemistry and morphology of the solid electrolyte interphase on silicon nanowire lithium-ion battery anodes. *J. Power Sources* **189,** 1132–1140 (2009).
31. Ruffo, R., Hong, S. S., Chan, C. K., Huggins, R. A. & Cui, Y. Impedance analysis of silicon nanowire lithium ion battery anodes. *J. Phys. Chem. C* **113,** 11390–11398 (2009).
32. Szczech, J. R. & Jin, S. Nanostructured silicon for high capacity lithium battery anodes. *Energy Environ. Sci.* **4,** 56–72 (2011).
33. Greiner, A. & Wendorff, J. H. Electrospinning: a fascinating method for the preparation of ultrathin fibres. *Angew. Chem. Int. Ed.* **46,** 5670–5703 (2007).
34. Li, D. & Xia, Y. N. Electrospinning of nanofibers: reinventing the wheel? *Adv. Mater.* **16,** 1151–1170 (2004).

Acknowledgements

This work was partially supported by the Assistant Secretary for Energy Efficiency and Renewable Energy, Office of Vehicle Technologies of the US Department of Energy (contract no. DE-AC02-05CH11231), and the Batteries for Advanced Transportation Technologies (BATT) Program (subcontract no. 6951379). This work is also partially supported by the SLAC National Accelerator Laboratory LDRD project. Y.C. acknowledges support from the King Abdullah University of Science and Technology (KAUST) Investigator Award (no. KUS-l1-001-12). G.C. acknowledges support from the Agency of Science, Technology and Research Singapore (A*STAR) National Science Scholarship. M.T.M. acknowledges support from the Stanford Graduate Fellowship, the National Science Foundation Graduate Fellowship and the National Defense Science and Engineering Graduate Fellowship.

Author contributions

H.W. and Y.C. conceived the idea. H.W., G.C. and Y.Y. carried out materials fabrication and electrochemical tests. J.W.C. and M.T.M. performed TEM measurements. I.R. and H.W. designed and carried out the simulations and analysed data. A.J performed Auger measurements. H.W. and Y.C. co-wrote the paper. All authors discussed the results and commented on the manuscript.

Additional information

The authors declare no competing financial interests. Supplementary information accompanies this paper at www.nature.com/naturenanotechnology. Reprints and permission information is available online at http://www.nature.com/reprints. Correspondence and requests for materials should be addressed to Y.C.